ORIGINAL RESEARCH ARTICLE

The Influence of Overall Texture on the Grain Boundary Network in an AZ31 Alloy

HOSSEIN BELADI, ALIREZA GHADERI, VAHID TARI, ANTHONY D. ROLLETT, and GREGORY S. ROHRER

Three samples of an AZ31 alloy with distinct textures were produced through chill casting, hot extrusion and hot rolling. The as-cast material exhibited a relatively random texture, while the hot extruded and hot rolled materials displayed {*hki*0} prism and (0001) basal textures, respectively. This also led to significant differences in the characteristics of their grain boundary networks (*i.e.*, the distribution of misorientations and plane orientations). The misorientation angle distribution of as-cast condition was similar to a random distribution. However, the other processing routes were significantly different from random, displaying a pronounced peak at ~ 30 deg misorientation angle, beyond which the distribution differed depending on the processing condition. Synthetically generated orientations belonging to each texture had misorientation angle distributions comparable to those measured for each processing route. This confirmed that the texture characteristics dictate the population of boundary misorientations. The distribution of grain boundary planes was anisotropic for all conditions, though the extent of anisotropy and their distribution characteristics depended on the processing route. It appeared that the relative areas of the grain boundary planes are largely influenced by the characteristics of the overall texture, where the hot rolling process promoted the (0001) basal plane orientation, while the {*hki*0} prismatic plane orientation, which does not necessarily have low energy, was dominant for the hot extrusion condition.

HOSSEIN BELADI is with the Institute for Frontier Materials, Deakin University, Geelong, Victoria 3216, Australia. Contact e-mail: hossein.beladi@deakin.edu.au ALIREZA GHADERI is with the Institute for Frontier Materials, Deakin University, Geelong, Australia, and also with the 3M, St Paul, USA. VAHID TARI is with the ATI Specialty Materials, Monroe, NC, 28111. ANTHONY D. ROLLETT and GREGORY S. ROHRER are with the Department of Materials Science and Engineering, Carnegie Mellon University, Pittsburgh, PA 15213-3890

Manuscript submitted December 4, 2024; accepted March 16, 2025.

Article published online March 27, 2025

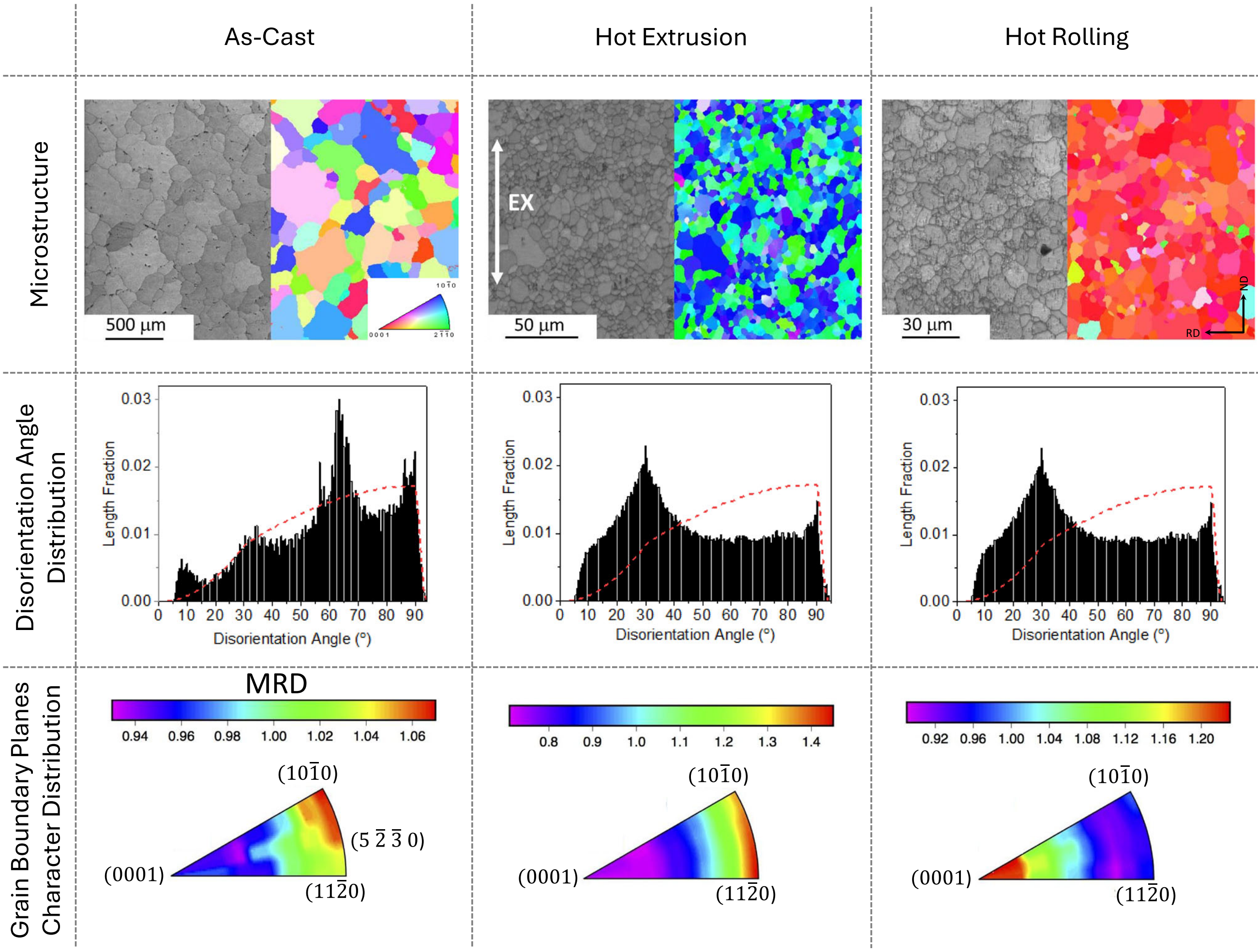

https://doi.org/10.1007/s11661-025-07754-z

I. INTRODUCTION

MAGNESIUM alloys are widely used for applications requiring low density combined with moderate strength (*e.g.*, automotive). However, they have low formability/ductility at ambient temperature due to the limited active slip systems (*i.e.*, non-basal slip) operating upon straining.[1,2] In turn, this promotes mechanical twinning as a dominant deformation mechanism in Mg alloys.[2] The grain boundaries appear as preferential sites for mechanical twinning nucleation because they are comprised of dislocation/defect aggregates and the presence of an abrupt change in orientation leads to high stress concentrations to maintain compatibility upon straining.[3]

Grain boundaries have anisotropic characteristics, defined by the atomic structure between two adjoining grains and the grain boundary plane character.[4–6] Hence, the propensity of mechanical twinning nucleation differs among different grain boundaries, depending on their characteristics.[3,7,8] For hexagonal close-packed materials (*e.g.*, Mg[8] and Ti[3] alloys), it was demonstrated that the mechanical twins largely nucleate on boundaries with low misorientation angles in a range of 5–10 deg, beyond which the propensity of mechanical twinning nucleation progressively decreases to such an extent that they are barely observed at boundaries with misorientation angles higher than 50 deg.[8] This suggests that the formability of magnesium alloys (*i.e.*, retarding the mechanical twinning formation) can, to some extent, be manipulated through control of their grain boundary network, a principle known as grain boundary engineering.

The concept of grain boundary engineering was introduced in mid-1980 s, largely focusing on austenitic metals having the face centred cubic structure.[9] Since then, several approaches have been developed to design grain boundary networks in a wide range of polycrystalline materials and ultimately enhance their material performance. These approaches consisted of iterative recrystallisation,[10] changing the mechanism of phase transformation (*i.e.*, diffusion vs shear),[11–13] varying alloy composition,[10,11,14] utilising variant selection,[11,14–16] and overall texture modification.[13,17–21] Among these methods, the influence of overall orientation texture is the most applicable to magnesium alloys, as they are readily manufactured through different processing routes, ultimately altering their overall texture. However, it is not clear how the change in the overall orientation texture alters the grain boundary network of magnesium alloys.

The current investigation examined the impact of overall texture on the characteristics of the grain boundary networks (*i.e.*, the distribution of misorientations and plane orientation) in an AZ31 Mg alloy. Here, the alloy was produced through different routes, namely chill casting, hot extrusion and hot rolling, leading to three distinct overall textures. The grain boundary characteristics produced by different processing conditions were evaluated using electron backscatter diffraction along with the automated stereological grain boundary interpretation known as the five-parameter characterisation method.[6] The results were then interpreted using a calculation of the misorientation angle distribution resulting from synthetically generated orientations for a given overall texture.

II. EXPERIMENTAL PROCEDURE

An AZ31 magnesium alloy with a nominal composition of Mg–2.8 Al–0.83 Zn–0.45 Mn (in wt pct) was received in different forms, namely cast ingot and 5 mm thick hot rolled plate. The latter is typically produced at a temperature range of 300 °C to 450 °C at a reduction of 10–30 pct per pass.[22] The hot rolled plate was used in the as-received condition, hereafter called the hot-rolled sample. However, the former was subjected to two different processing routes, as follows:

– *Chill Casting:* The as-received cast ingot was remelted at 800 °C in a stainless-steel crucible, and then solidified in a chill mould with a dimension of $100 \times 20 \times 20$ mm^3 under argon gas, to reduce the formation of columnar dendrites upon solidification. The cast block was scalped to remove the chill zone near the casting surface. The material was then annealed at 450 °C for 16 h under inert gas (hereafter called the as-cast condition) to remove any mechanical twins, which might be introduced because of stress associated with contraction/shrinkage during the solidification.

– *Extrusion:* The as-received cast ingot was machined into a rod having a 30 mm diameter and 20 mm length, which was then subjected to hot extrusion using a laboratory extrusion rig embedded in a servo-hydraulic testing frame having a load capacity of 350 kN. The hot extrusion was performed at 350 °C temperature and a ram speed of 0.1 mm/s to obtain an extruded rod with final diameter of 8 mm.

Electron backscatter diffraction (EBSD) was employed to characterise the microstructures produced with the different processing routes. The EBSD samples were prepared using standard mechanical grinding and polishing procedures. They were further polished using a colloidal alumina slurry solution. The microscope was operated at 20 kV and 4 nA current using different step sizes, depending on the microstructure characteristics (*i.e.*, grain size). For each processing route, several EBSD maps were obtained using a FEI Quanta 3D FEG SEM/FIB instrument. For the as-cast condition, multiple samples were prepared from different parts of the annealed block to provide a good statistical representation of the microstructure throughout the thickness. For the hot rolled condition, two perpendicular cross sections were taken: one in the rolling direction and normal direction plane (RD-ND), and the other in the rolling direction and transverse direction plane (RD-TD) for microstructure characterisation. EBSD was also conducted on two perpendicular cross sections of the extruded sample, namely parallel to the extrusion direction (ED-TD) and perpendicular to the extrusion direction (TD-ND). Roughly equal amounts of EBSD data were collected from two perpendicular cross-sections for the rolled and extruded conditions to diminish the texture bias introduced in the measurement of the grain boundary plane distribution using the five-parameter characterisation approach, as described below. The EBSD map parameters were summarised in Table I for different processing conditions. The EBSD average confidence index varied between 0.6 and 0.7 depending on the microstructure characteristics developed for different processing routines.

Table I. EBSD Condition of AZ31 Alloy Produced Through Different Processing Routes

Condition	Grain Size (μm)	Step Size (μm)	EBSD Area	Total Line Segments
As-Cast	154 ± 5	5	2400×2400 μm^2 $\times$ 220	209,220
Extruded	3.9 ± 0.6	0.2	128×128 μm^2 $\times$ 42	407,172
Rolled	5.9 ± 1.1	0.2	183×183 μm^2 $\times$ 53	390,178

The characterisation of grain boundary interfaces in polycrystalline materials requires five independent macroscopic parameters: three for lattice misorientation and two for the boundary plane orientation.[6] The lattice misorientation is defined by Euler angles (φ_1, Φ, φ_2) or an angle/axis pair (θ/[uvw]), which are defined using conventional EBSD analysis. Each boundary segment corresponds to the grain boundary trace on the surface plane. The only remaining parameter is the inclination of the boundary plane relative to the surface to fully determine the boundary plane orientation. If enough grain boundary traces are collected for a given angle/axis pair, the grain boundary plane distribution can be determined using a stereological approach.[6] Here, it is expected that each grain boundary line segment is orthogonal to its boundary plane normal. Therefore, all possible plane normals for a given boundary segment lie on a great circle perpendicular to it on a stereographic projection. By measuring multiple boundary segments with a fixed lattice misorientation, the most probable plane/s appears as peak/s in the distribution, while less probable ones are observed less frequently and can be removed as background.[6]

The TexSEM Laboratories (TSL) software was used to acquire the EBSD data and perform the data post-processing. For grain boundary plane characterisation, boundary lines/traces were obtained from EBSD data after conducting several data post-processing functions in the TSL software, namely grain dilation clean-up, single orientation designation for each grain, and grain boundary reconstruction.[12] The clean-up routine was performed to minimize ambiguous data from the orientation map, which, on average, altered less than 4 pct of original data points. The grain boundary reconstruction function smoothed uneven boundaries using a boundary deviation limit of 2 times the step size to extract boundary segments for each processing condition. Owing to the low crystal symmetry in the hexagonal crystal structure (*i.e.*, AZ31 Mg alloy), a minimum of 200,000 boundary line segments were collected for each processing routine (Table I) to correctly measure the grain boundary plane distribution using the five-parameter characterisation approach.[6] The current measurement had a resolution of 10 deg. The Atex post-processing software[23] was used to plot the overall texture at different conditions.

III. RESULTS

The microstructure of the as-cast specimen after heat treatment was relatively coarse with equiaxed grains having an average size of 154 $\pm$ 5 μm (Figure 1(a)). The heat treatment had removed any tension twins formed because of the shrinkage taking place during the solidification.[24] The misorientation angle distribution exhibited several maxima at the misorientation angle range of 5–10 deg, 30–35 deg, 55–65 deg and 85–90 deg (Figure 2(a)). The distribution deviated somewhat from the ideal random distribution, even though the overall texture was relatively weak with an intensity of ~ 1.8 multiples of a random distribution (MRD, Figure 2). The misorientation axis distribution at the peak positions largely exhibited maxima at [0001], $[11\bar{2}0]$ and/or $[10\bar{1}0]$ (Figure 2(a)). The misorientation axis distribution at 10 deg had a maximum at [0001] spreading towards $[10\bar{1}0]$. At 30 deg, the distribution displayed a maximum at $[10\bar{1}0]$. The misorientation axis distribution at 65 deg revealed a peak near the $[11\bar{2}0]$ position. A single peak was also observed at $[11\bar{2}0]$ for the misorientation axis distribution at 90 deg (Figure 2(a)).

The hot extruded AZ31 alloy revealed fine equiaxed grains (*i.e.*, 3.9 $\pm$ 0.6 μm, Figure 1(b)), displaying a typical extrusion texture having ~ 6 MRD intensity, where the extrusion direction is largely perpendicular to the basal poles and parallel to the $\{10\bar{1}0\}$ and $\{11\bar{2}0\}$ poles (Figure 3(b)). In turn, the inverse pole figure showed a maximum at the $[11\bar{2}0]$ direction spreading towards the $[10\bar{1}0]$, with ~ 5.9 MRD intensity (Figure 3(c)). The misorientation angle distribution

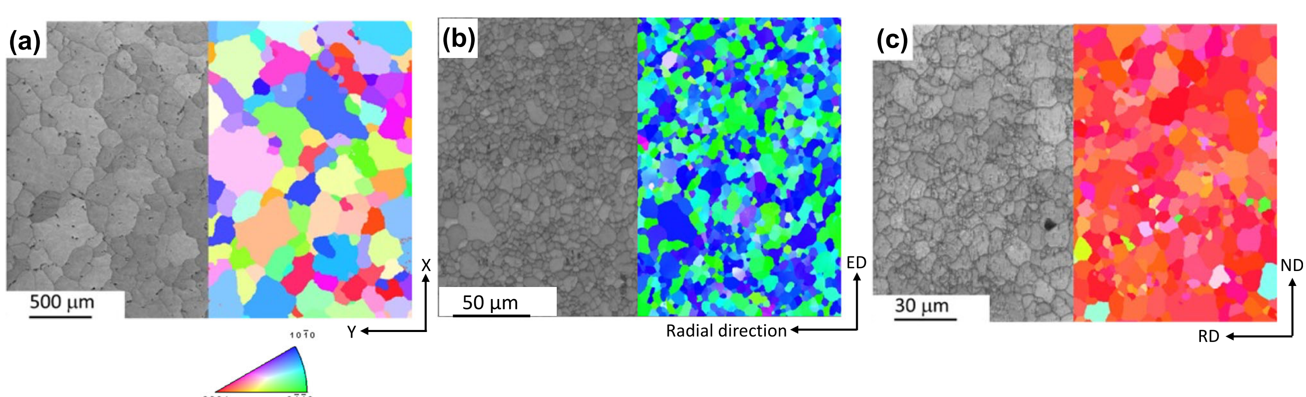

Fig. 1—EBSD band contrast and their corresponding IPF images of AZ31 produced through different processing routes: (*a*) as-cast, (*b*) hot extrusion and (*c*) hot rolling. The triangle inset in (a) is colour codes referring to the out of plane direction. X and Y in (a) are arbitrary directions, though the out of plane direction is parallel to the solidification direction. ED, RD, ND represent extrusion direction, rolling direction and normal direction, respectively.

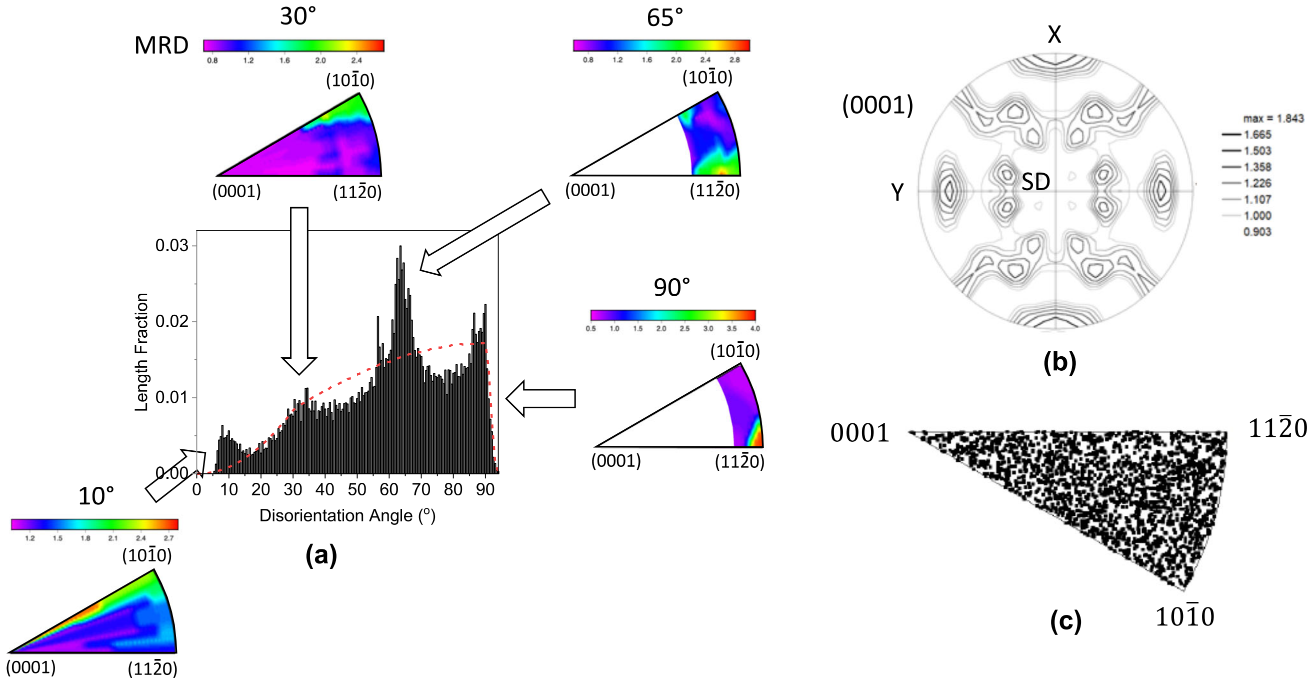

Fig. 2—(*a*) misorientation angle distribution of as-cast AZ31 alloy along with the misorientation axis distribution at the peaks. Dashed red line in (a) represents the random distribution of misorientation angle. The (0001) pole figure (*b*) reprinted with permission from Ref. [24] along with the inverse pole figure (*c*) of the as-cast AZ31 alloy. X and Y in (b) are arbitrary directions and SD represents the solidification direction. MRD represents multiples of a random distribution.

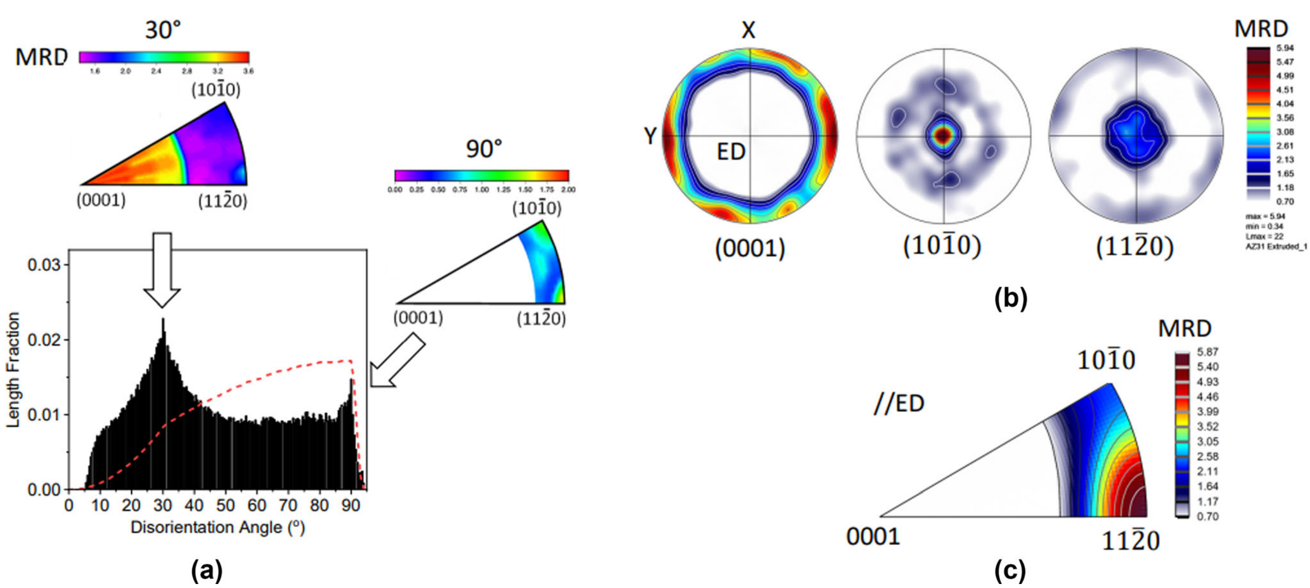

Fig. 3—(*a*) misorientation angle distribution of hot extruded AZ31 alloy along with the misorientation axis distribution at the peaks. Dashed red line in (a) represents the random distribution of misorientation angle. The pole figures (*b*) along with the inverse pole figure (*c*) of hot extruded AZ31 alloy. MRD represents multiples of a random distribution. ED is extrusion direction.

significantly deviated from the one expected for the ideal random distribution, revealing two peaks at ~ 30 and ~ 90 deg (Figure 3(a)). Interestingly, the misorientation angle was nearly a plateau between ~ 45 and ~ 85 deg. The misorientation axis distribution largely clustered at the [0001] for 30 deg and, $[10\bar{1}0]$ and $[11\bar{2}0]$ for 90 deg misorientation angle (Figure 3(a)).

The specimen produced by hot rolling had small grain size of 5.9 ± 1.1 μm with an equiaxed morphology (Figure 1(c)). The sample displayed a strong basal texture, where the normal direction was parallel to the basal plane, spreading by ~ 20 deg towards the rolling direction and having ~ 8.8 MRD intensity (Figure 4(b)). The inverse pole figure also exhibited a strong peak at

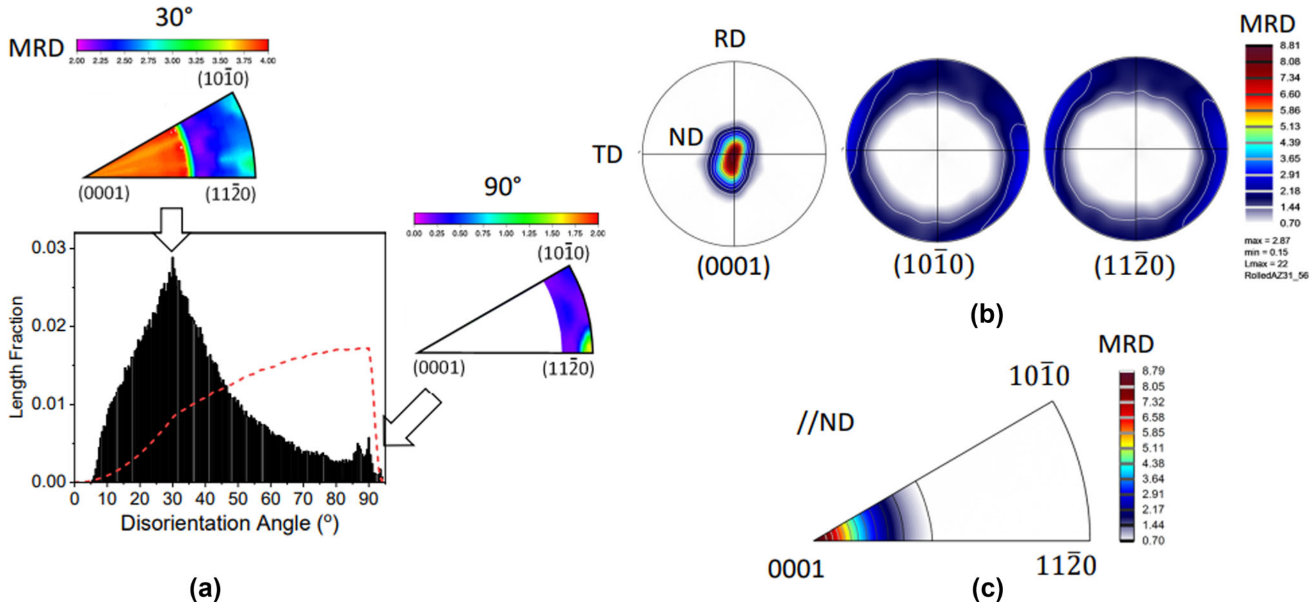

Fig. 4—(*a*) misorientation angle distribution of hot rolled AZ31 alloy along with the misorientation axis distribution at the peaks. Dashed red line in (a) represents the random distribution of misorientation angle. (*b*) the pole figures (b) along with the inverse pole figure (*c*) of hot rolled AZ31 alloy. MRD represents multiples of a random distribution. RD, TD and ND are rolling direction, transverse direction and normal direction, respectively.

[0001], having an intensity of ~ 8.8 MRD (Figure 4(c)). The population of misorientation angles increased continuously up to 30 deg, beyond which it progressively decreased up to a misorientation angle of ~ 85 deg. Thereafter, the misorientation angle displayed a rather weak peak at ~ 90 deg (Figure 4(a)). The corresponding misorientation axis distribution at 30 deg exhibited a somewhat diffuse peak at [0001] position, it was clustered at $\left[11\bar{2}0\right]$ for 90 deg misorientation angle (Figure 4(a)).

The grain boundary planes distribution was only drawn for $30°/\left[10\bar{1}0\right]$ and $90°/\left[11\bar{2}0\right]$ for the as-cast AZ31 alloy, since those related to other lattice misorientations have been already presented in.[24] The geometrically characteristic grain boundaries were also mapped for the corresponding lattice misorientations to define the character of the relevant boundary using the toolbox defined in.[25] At $30°/\left[10\bar{1}0\right]$, the grain boundary planes distribution showed a maximum close to the position of $\left(\bar{1}2\bar{1}1\right)$ plane with an intensity of ~ 6.8 MRD (Figures 5(a) and (d)). For $90°/\left[11\bar{2}0\right]$, the distribution displayed a peak with an intensity of ~ 7.2 MRD at the position of $\left(01\bar{1}1\right)$ plane orientation with twist character, considering an equivalent lattice misorientation outside of fundamental zone (Figures 5(c) and (g)).

For the hot extruded condition, the grain boundary plane distribution at 30°/[0001] exhibited multiple peaks with an intensity of ~ 5 MRD at the positions of the $\left\{11\bar{2}0\right\}$ and $\left\{10\bar{1}0\right\}$ prism planes, which differ by 30° about the [0001] misorientation axis (Figures 5(b) and (e)). This suggests that it has $\left(2\bar{1}\bar{1}0\right)//\left(10\bar{1}0\right)$ asymmetric tilt character, since the grain boundary planes are from distinct family. The grain boundary planes at the $90°/\left[11\bar{2}0\right]$ and $90°/\left[10\bar{1}0\right]$ misorientations did not have maxima greater than 2.5 MRD and were not considered significant to present.

For the hot rolled condition, the grain boundary plane distribution at 30°/[0001] misorientation showed a peak at the position of (0001) with ~ 5.8 MRD, suggesting pure twist character (*i.e.*, the misorientation axis and plane normal are parallel, Figures 5(b) and (f)). However, the distribution at $90°/\left[11\bar{2}0\right]$ exhibited two main peaks with ~ 5.1 MRD intensity at the $\left(1\bar{1}02\right)$ and $\left(\bar{1}102\right)$ planes, having symmetric tilt character, since both planes at the boundary belong to the same family (*i.e.*, $\left(1\bar{1}02\right)//\left(\bar{1}102\right)$, Figures 5(c) and (h)).

The grain boundary plane distribution, irrespective of misorientation, was plotted for all microstructures formed during the different processing routes (Figure 6). It appeared that the processing condition significantly affected the distribution. For the as-cast condition, the highest intensity was at $\left(10\bar{1}0\right)$ with 1.07 MRD, spreading towards the $\left(5\bar{2}\bar{3}0\right)$. The minimum intensity was 0.93 MRD at (0001). In general, the intensity difference was ~ 14 pct between the maximum and minimum positions in the distribution, indicating a relatively weak anisotropic distribution (Figure 6(a)).

For the hot extruded condition, the boundaries were largely terminated on $\{hki0\}$ prismatic planes with a maximum of 1.45 MRD at the $\left(11\bar{2}0\right)$ orientation, spreading towards the $\left(10\bar{1}0\right)$ orientation (Figure 6(b)). This confirms that the distribution of grain boundary plane orientations was anisotropic, because the $\{hki0\}$ prismatic plane population was 45 pct higher than anticipated in a random distribution.

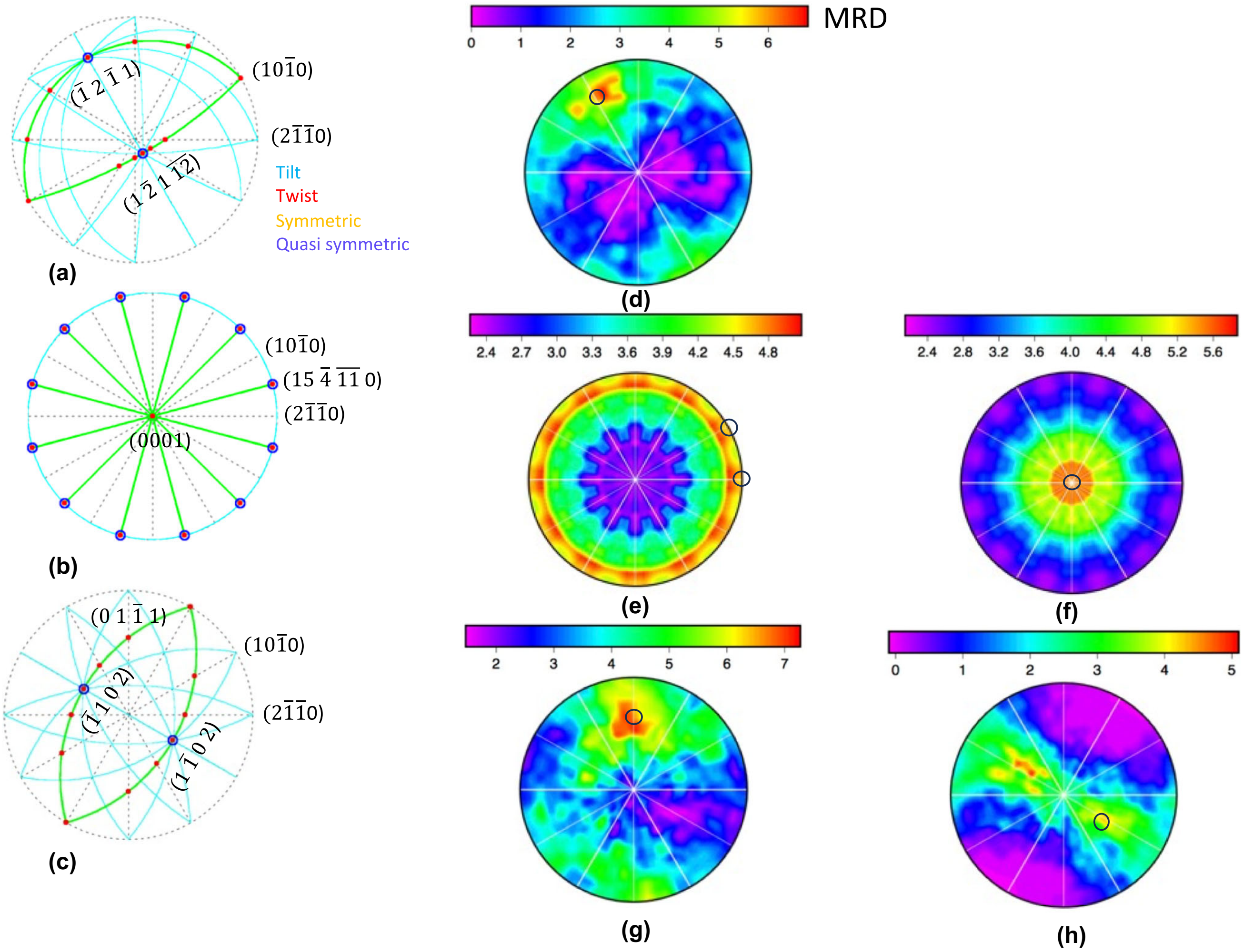

Fig. 5—The calculated locations of the geometrically characteristic boundaries [25] for lattice misorientations of (*a*) 30°/[10$\bar{1}$0], (*b*) 30°/[0001] and (*c*) 90°/[11$\bar{2}$0]. The distribution of grain boundary planes character for different lattice misorientations for microstructures produced through different processing routes: (*d*) 30°/[10$\bar{1}$0], as-cast, (*e*) 30°/[0001], hot extruded, (*f*) 30°/[0001], hot rolled, (*g*) 90°/[11$\bar{2}$0], as-cast, and (*h*) 90°/[11$\bar{2}$0], hot rolled. MRD represents multiples of a random distribution.

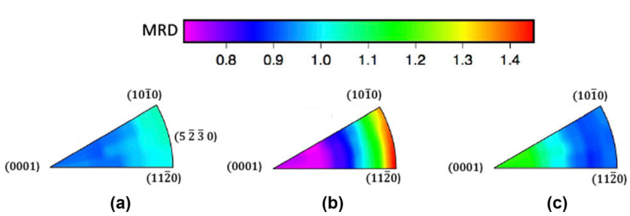

Fig. 6—The grain boundary planes character distribution ignoring misorientation for AZ31 alloy produced through different processing routes: (*a*) as-cast reprinted with permission from Ref. [24], (*b*) hot extruded and (*c*) hot rolled. MRD is multiples of a random distribution.

For the hot rolled condition, the grain boundary plane distribution was significantly different compared with other conditions, displaying the highest intensity of 1.22 MRD at the (0001) basal plane orientation (Figure 6(c)). The distribution was anisotropic, having the population of (0001) basal plane orientation 22 pct larger than expected from a random distribution. By contrast, the distribution exhibited a minimum at the {*hki*0} prismatic planes.

IV. DISCUSSION

The current result demonstrates that the grain boundary network (*i.e.*, the distribution of misorientations and plane grain boundary orientations) is significantly affected by the processing route for AZ31 Mg alloy (Figures 2 through 6). There are a wide range of parameters affecting the boundary network in polycrystalline materials, namely chemical composition,[10,11,14] phase transformation mechanism,[11–13,26] initial grain size,[27] and crystallographic texture.[13,17–21] The chemical composition and phase transformation mechanism can be excluded here, because the composition is similar for all different processing routes and the material did not undergo any phase transformation during processing. However, the grain size of the as-cast condition is much greater than others, although they are relatively similar for the hot extruded and hot rolled conditions (Table I), where they have distinct grain boundary plane distributions (Figure 6). This suggests that the grain size is not the most important factor determining the grain boundary network in the current study. However, the overall orientation texture is significantly different due to varying processing routes.

The overall texture significantly affects the population of grain boundaries in polycrystalline materials.[13,17–21] This was largely demonstrated for materials with the cubic crystal structure, where the introduction of a given crystallographic fibre texture through the processing route promotes specific boundary type/s at the expense of others.[20,21] The current observation also suggests that altering the material processing route leads to unique overall texture, which influences the grain boundary network (Figures 2 through 6). The overall texture characteristics depend on the deformation mode and alloying content (*i.e.*, c/a ratio).[28] Hot extrusion leads to the enhancement of prism orientations, where the extrusion direction is parallel to the $\{hki0\}$ orientations (Figure 3). However, the hot rolling promotes the (0001) basal orientation (*i.e.*, ND//(0001), Figure 4).

In both the hot extrusion and hot rolling processes, there is a dominant peak at the position of ~ 30 deg (Figures 3 and 4). However, the misorientation angle distribution varies beyond 30 deg, depending on the processing route. To investigate the influence of overall orientation texture on the misorientation angle distribution, we utilised a similar approach recently used by our group to assess the role of γ-fibre and θ-fibre texture on the misorientation angle distribution in fully ferritic IF-steel[20] and fully austenitic Ni-30Fe alloy.[21] Considering the c/a ratio of the AZ31 alloy (*i.e.*, 1.6247[29]), this is close to the ideal c/a ratio of 1.633, expected to largely produce the ND//(0001) fibre in rolling.[30] Here, 5000 orientations are randomly selected along the ND//(0001) fibre, where these orientations have their φ_1 and φ_2 angles arbitrarily designated, varying from 0 to 360 deg, with fixed ϕ angle of 0 deg (Figure 7(a)). The disorientation angle resulted from the two orientations, located along the ND//(0001) fibre is calculated using the Equation [1].

$$\Delta g_{ij} = (O_m g_j)(O_l g_i)^{-1} \quad [1]$$

where Δg_{ij} is disorientation angle and g_i and g_j are ith and jth orientation of every two adjacent sets, respectively, both changing from 1 to 5000. O_l and O_m, in turn, represent the 12 hexagonal symmetry operators for g_i and g_j. The disorientation refers to the minimum angle and is calculated from the set of 288 equivalent misorientations, considering switching symmetry. Here, it is assumed that the hypothetical orientations intersect each other only one time throughout the calculation, with i equal or smaller than j. Furthermore, the boundary formed from the intersection of every orientation pair has a constant length for each calculated boundary. Hence, it does not influence the resultant disorientation angle distribution. The distribution was discretised with a bin width of 1 deg. The resultant disorientation angles display a uniform distribution, restricted in the range of 0 to 30 deg, which covers all distinguishable rotation angles about the [0001] (Figure 7(a)). This signifies that the manifestation of strong basal fibre texture enhances the presence of all disorientation angles ranging from 0 to 30 deg with an

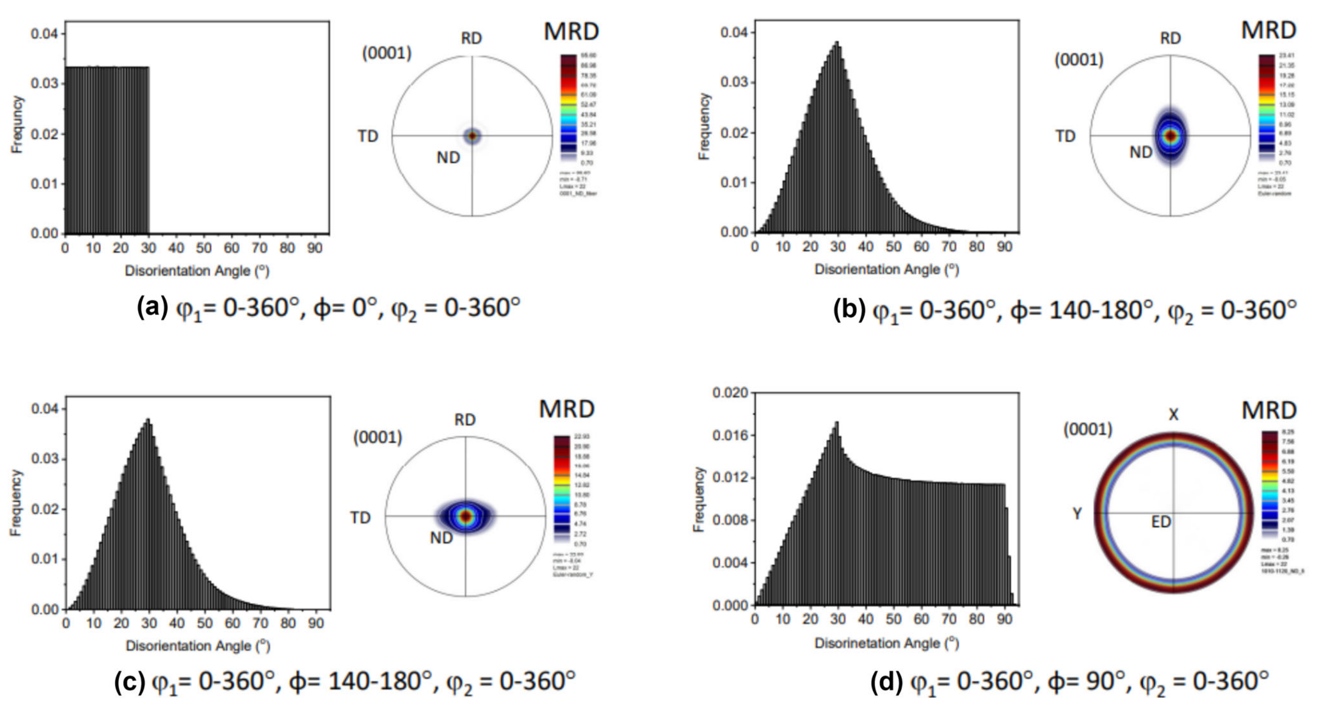

Fig. 7—Disorientation angle distribution resulted from the impingement of each pair of 5000 synthetically chosen orientations within different Euler angles ranges and their corresponding (0001) pole figures.

equal probability, resulting in a uniform/flat distribution. The result of this calculation significantly differs from the current experimental measurement, where there is a maximum in the misorientation angle distribution at 30 deg (Figures 4(a) and 7(a)). This discrepancy could be due to the difference in the overall texture of the hot rolled AZ31 alloy from the ideal basal fibre, where the peak was spread from the normal direction towards the rolling direction by ~ 20 deg (Figure 4(b)). To synthetically generate the experimental texture, the 5000 hypothetical orientations are arbitrarily selected from Euler angles space of $\varphi_1 = 0$ through 360 deg, $\phi = 140$ through 180 deg and $\varphi_2 = 0$ through 360 deg, so that the overall texture appears as an ellipse spread 20 deg towards RD. The calculated disorientation angle distribution shows a single peak at the 30 deg disorientation angle, progressively reducing with the disorientation angle (Figure 7(b)). This closely matches with the measured experimental data (Figure 4). The calculation was also performed for the material with a pole in their overall texture elongated towards the TD direction, representing the materials with $c/a < 1.633$ such as Ti. The calculation exhibited a similar trend with a pronounced peak at 30 deg (Figure 7(c)). A similar disorientation angle distribution was also reported by others for different hexagonal materials (Zr,[31] Ti[32]) subjected to the hot rolling and/or recrystallisation.

To evaluate the influence of hot extrusion texture on the disorientation angle distribution, 5000 hypothetical orientations are randomly chosen from the Euler angles space of $\varphi_1 = 0$ through 360 deg, $\phi = 90$ deg and $\varphi_2 = 0$ through 360 deg. The calculated data exhibit a sharp increase in the disorientation angle up to 30 deg beyond which it reduces with the disorientation angle up to 45 deg. Afterwards, the distribution became flat up to 90 deg, where it sharply reduces (Figure 7(d)). This closely matches the experimentally measured distribution, although some fluctuations appeared in the experimental result, which can be due to the deviation in the measured overall texture from the ideal assumed condition (Figure 3).

The microstructure of both hot extruded and hot rolled conditions was largely equiaxed grains surrounded by both low and high angle boundaries (Figure 1). Therefore, the presence of high fraction of low angle boundaries is most likely due to the overall texture, rather than the presence of deformed grains (incomplete recrystallisation). In other words, the hot deformed microstructure in both hot extruded and hot rolled conditions has undergone static/metadynamic recrystallisation upon post-deformation air-cooling, leading to equiaxed grains.

The current observations also demonstrate that the grain boundary plane distribution is anisotropic (Figure 6), which is consistent with the other reports for a wide range of polycrystalline materials.[4,5,33,34] However, the extent of anisotropy and the distribution characteristics were significantly affected by the processing route. It has been demonstrated that an inverse relationship exists between the relative areas of grain boundaries and their energies for microstructures formed through normal grain growth, both in simulations[35–38] and experimental measurements.[4,5,39,40] In fact, the grain boundaries which are frequently observed exhibit the least energy and vice versa. Here, the interplanar spacing (*i.e.*, d_{hkil}) of the boundary planes is employed as a proxy for the relative grain boundary energy,[41,42] due to a lack of information regarding the grain boundary energies of Mg alloys. Based on this model, a boundary consisting of planes with large interplanar spacing refers to a low energy boundary, as they are fairly flat and smooth with limited numbers of broken bonds. Therefore, they probably match better with the neighboring plane, consequently reducing repulsion forces at the boundary and lowering the grain boundary energy.[41,42] By contrast, smaller interplanar spacings imply more broken bonds and rougher planes, which ultimately reduce the atomic density of boundary structure, leading to higher boundary energy. Table II listed the interplanar spacings of planes representing maxima in the distributions measured in the present work.

Interestingly, the link between the populations and the interplanar spacing does not follow a similar trend for all processing conditions. For the hot rolled condition, a direct correlation appears between the populations and the interplanar spacing, where the (0001) basal plane with the highest population has the largest interplanar spacing (2.6 Å) among all boundary planes (Figure 6(c) and Table II). However, no direct trend is observed between populations and interplanar spacing for the as-cast and hot extruded conditions (Figures 6(a) and (b) and Table II). Here, the $\{hki0\}$ prismatic planes (*e.g.*, $(10\bar{1}0)$, $(5\bar{2}\bar{3}0)$ and $(11\bar{2}0)$) are the most frequent planes, though their interplanar spacings are lower than for the (0001) basal plane with minimum population (Table II). This confirms that the grain boundary energy is not the most important factor determining the grain boundary plane distribution when the processing route leaves an imprint on the microstructure.

The main difference among these microstructures is the processing condition, which leads to different overall textures. There is ample evidence that the overall texture has a direct impact on the relative areas of grain boundaries.[20,21,44] For example, the promotion of γ-fibre (*i.e.*, $(111)//ND$) in IF steel with a fully ferritic structure enhances the boundaries with a (111) plane orientation, having a greater energy compared with the (110) close packed plane orientation (*i.e.*, low energy plane).[20] Similarly, the increase in the strength of θ-fibre (*i.e.*, $(001)//ND$)) in a Ni-30Fe alloy leads to the enhancement of boundaries terminated at (001) rather than the (111) close packed plane in materials with the face centred cubic structure.[21] This is similar to the current observation, where the grain boundary plane distribution is closely matched with the overall texture for both hot extrusion and hot rolling conditions. For example, the hot extrusion condition enhances the relative areas of boundaries that terminate at $\{hki0\}$ prismatic plane orientations (Figures 3(c) and 6(b)). A similar distribution was observed for α-Ti, though the anisotropy was relatively weak.[45] In terms of the hot rolling condition, the promotion of the (0001) basal

Table II. The Interplanar Spacings (d_{hkil}) for Different Planes Observed in Figs. 5 and 6

Plane Orientation	Interplanar Spacing ($\dot{A}$)
(0001)	2.60
$(10\bar{1}0)$	1.86 or 0.93[a]
$(11\bar{2}0)$	1.6
$(5\bar{2}\bar{3}0)$	0.43 or 0.21[a]
$(\bar{1}2\bar{1}1)$	0.77
$(01\bar{1}1)$	2.44 or 0.41[a]
$(1\bar{1}02)$	1.27 or 0.63[a]
$(\bar{1}102)$	1.27 or 0.63[a]

[a]Considering the structure factor where the plane passing through an additional atom.[43]

fibre leads to the (0001) basal planes, which coincide with the low energy position based on the interplanar spacing criterion (Figures 4(c), 6(c) and Table II). However, in this case the large relative areas of (0001) planes are a consequence of the processing and are not likely to be energetically driven. Regarding the as-cast condition, a relatively stronger $\{hki0\}$ prismatic plane orientations in the distribution (Figure 6(a)) could be explained due to the existence of remaining columnar grains, developed during the growth of dendrites with their six secondary arms being along the $\langle 11\bar{2}0\rangle$ direction upon solidification.[46] However, the orientations of lateral columnar surfaces are expected to be perpendicular to the $\langle 11\bar{2}0\rangle$ growth direction (*i.e.*, $\{1\bar{1}00\}$ and (000 1)). This is contradicted by the observation that the grain boundary plane distribution maximizes at $\{1\bar{1}00\}$, but not (0001).[24]

The current result demonstrates that the hot rolling condition has the highest population of low angle grain boundaries among different processing routes (Figures 2 through 4). Based on the simulation result presented in,[8] it is expected that the grain boundary network developed in AZ31 alloy produced through the hot rolling is more prone to mechanical twinning nucleation on grain boundaries, considering the link between grain boundary character (*i.e.*, misorientation angle of < 10 deg[8]) and mechanical twinning.

V. CONCLUSIONS

In the current investigation, the role of processing route (*i.e.*, chill casting, hot extrusion and hot rolling) on the overall orientation texture and the characteristics of grain boundary network was investigated for an AZ31 alloy. The observations lead to the following conclusions:

(1) The processing route altered the overall texture, revealing random texture in the as-cast condition, although the $\{hki0\}$ prism and the (0001) basal textures were dominant after hot extrusion and hot rolling, respectively.

(2) The change in the overall texture appeared to control the misorientation angle distribution, where the as-cast condition displayed a relatively random distribution. However, the distribution deviated significantly from the random case for both the hot extruded and hot rolled conditions, displaying pronounced peaks at ~ 30 deg. Computed misorientation angle distributions based on simulations confirmed the role of texture in determining these distributions.

(3) The distribution of grain boundary planes was somewhat anisotropic for the as-cast condition, showing stronger $\{hki0\}$ prismatic plane orientations. In comparison, the anisotropy became much stronger for both hot extruded and hot rolled materials.

(4) The characteristics of overall texture appeared to strongly influence the relative areas of grain boundary planes. The basal texture in the hot rolled condition enhanced the occurrence of the (0001) basal plane orientation, but the $\{hki0\}$ prismatic plane orientations appeared more frequently in the hot extruded material, despite having a relatively higher energy than the (0001) basal plane.

ACKNOWLEDGMENTS

Deakin University's Advanced Characterisation Facility is acknowledged for use of the EBSD instruments.

FUNDING

Open Access funding enabled and organized by CAUL and its Member Institutions.

CONFLICT OF INTEREST

On behalf of all authors, the corresponding author states that there is no conflict of interest.

REFERENCES

1. M.H. Yoo: *Metall. Trans. A*, 1981, vol. 12, pp. 409–18.
2. M.A. Meyers, O. Vohringer, and V.A. Lubarda: *Acta Mater.*, 2001, vol. 49, pp. 4025–39.
3. L. Capolungo, P.E. Marshall, R.J. McCabe, I.J. Beyerlein, and C.N. Tome: *Acta Mater.*, 2009, vol. 57, pp. 6047–56.
4. H. Beladi, N.T. Nuhfer, and G.S. Rohrer: *Acta Mater.*, 2014, vol. 70, pp. 281–89.
5. H. Beladi and G.S. Rohrer: *Acta Mater.*, 2013, vol. 61, pp. 1404–12.
6. G.S. Rohrer, D.M. Saylor, B.E. Dasher, B.L. Adams, A.D. Rollett, and P. Wynblatt: *Z. Met.*, 2004, vol. 95, pp. 197–214.
7. V. Shterner, I.B. Timokhina, A.D. Rollett, and H. Beladi: *Metall. and Mater. Trans. A*, 2018, vol. 49, pp. 2597–2611.
8. I.J. Beyerlein, L. Capolungo, P.E. Marshall, R.J. McCabe, and C.N. Tome: *Philos. Mag.*, 2010, vol. 90, pp. 2161–90.
9. T. Watanabe: *Trans. Japan Inst. Metals*, 1986, vol. 27, p. 73.
10. V. Randle: *Acta Mater.*, 1999, vol. 47, pp. 4187–96.
11. E. Farabi, V. Tari, P.D. Hodgson, G.S. Rohrer, and H. Beladi: *J. Mater. Sci.*, 2020, vol. 55, pp. 15299–5321.
12. H. Beladi, G.S. Rohrer, A.D. Rollett, V. Tari, and P.D. Hodgson: *Acta Mater.*, 2014, vol. 63, pp. 86–98.
13. H. Beladi and G.S. Rohrer: *Metall. and Mater. Trans. A*, 2017, vol. 48, pp. 2781–90.
14. V. Govindaraj, E. Farabi, S. Kada, P.D. Hodgson, R. Singh, G.S. Rohrer, and H. Beladi: *J. Alloys Compd.*, 2021, vol. 886, p. 161333.
15. A. Mirzaei, R. Ghaderi, P.D. Hodgson, X. Ma, G.S. Rohrer, and H. Beladi: *J. Mater. Sci.*, 2022, vol. 57, pp. 8904–23.
16. A. Mirzaei, P.D. Hodgson, X. Ma, V. Peterson, E. Farabi, G.S. Rohrer, and H. Beladi: *Mater. Sci. and Eng. A*, 2024, vol. 889, p. 145793.
17. H. Beladi, E. Farabi, P.D. Hodgson, M.R. Barnett, G.S. Rohrer, and D. Fabijanic: *Phil. Mag.*, 2022, vol. 102, pp. 618–33.
18. D.A. West and B.L. Adams: *Metall. Mater. Trans. A*, 1997, vol. 28, pp. 229–36.
19. R.E. Garcia and M.D. Vaudin: *Acta Mater.*, 2007, vol. 55, pp. 5728–35.
20. H. Beladi, V. Tari, A.D. Rollett, and G.S. Rohrer: *Scripta Mater.*, 2023, vol. 222, p. 115042.
21. H. Beladi, Q. Chao, V. Tari, A.D. Rollett, and G.S. Rohrer: *Mater. Charac.*, 2023, vol. 197, p. 112708.
22. Y. Wu and R. Zhu: *J. Mater. Eng. and Perfor.*, 2019, vol. 28, pp. 6182–91.
23. B. Beausir and J.-J. Fundenberger: Analysis tools for electron and X-ray diffraction, ATEX—software, Université de Lorraine-Metz, 2017. www.atex-software.eu.
24. H. Beladi, A. Ghaderi, and G.S. Rohrer: *Phil. Mag.*, 2020, vol. 100, pp. 456–66.
25. K. Glowinski and A. Morawiec: A toolbox for geometric grain boundary characterization, in *Proceedings of the 1st International Conference on 3D Material Sciences*. Springer, Cham, 2012, pp. 119–24.
26. N. Haghdadi, P. Cizek, P.D. Hodgson, V. Tari, G.S. Rohrer, and H. Beladi: *Acta Mater.*, 2018, vol. 145, pp. 196–209.
27. T. Liu, S. Xia, H. Li, B. Zhou, Q. Bai, C. Su, and Z. Cai: *J. Mater. Res.*, 2013, vol. 28, pp. 1165–76.
28. G. Gottstein and T. Al-Samman: *Mater. Sci. Forum*, 2005, vol. 495–497, pp. 623–32.
29. T.H. Rriyanto, A. Insani, R. Muslih, and Bharoto: *IOP Conf. Series: J. Phys.*, 2020, vol. 1436, p. 012061.
30. Y.N. Wang and J.C. Huang: *Mater. Chem. and Phys.*, 2003, vol. 81, pp. 11–26.
31. N. Bozzolo, F. Gerspach, G. Sawina, F. Wagner, Accuracy of orientation function determination based on EBSD data—a case study of a recrystallized low alloyed Zr sheet, J. of Microscopy, 227 (2207), pp. 275-83.
32. N. Bozzolo, N. Dewobroto, T. Grosdidier, and F. Wagner: *Mater. Sci. and Eng. A*, 2005, vol. 397, pp. 346–55.
33. D.M. Saylor, B. Dasher, Y. Pang, H.M. Miller, P. Wynblatt, A.D. Rollett, and G.S. Rohrer: *J. Am. Ceram. Soc.*, 2004, vol. 87, pp. 724–26.
34. H. Beladi and G.S. Rohrer: *Metall. Mater. Trans. A*, 2013, vol. 44, pp. 115–24.
35. J. Gruber, D.C. George, A.P. Kuprat, G.S. Rohrer, and A.D. Rollett: *Scripta Mater.*, 2005, vol. 53, pp. 351–55.
36. G.S. Rohrer, J. Gruber, and A.D. Rollett: A model for the origin of anisotropic grain boundary character distributions in polycrystalline materials, in *Applications of Texture Analysis, in Ceramic Transactions of Applications of Texture Analysis*, vol. 201, A.D. Rollett, ed., John Wiley, Hoboken, 2009, pp. 343–54.
37. J. Gruber, G.S. Rohrer, and A.D. Rollett: *Acta Mater.*, 2010, vol. 58, pp. 14–19.
38. J.D. Nino and O.K. Johnson: *Comp. Mater. Sci.*, 2023, vol. 217, p. 111879.
39. S.J. Dillon and G.S. Rohrer: *J. Am. Ceram. Soc.*, 2009, vol. 92, pp. 1580–85.
40. J. Li, S.J. Dillon, and G.S. Rohrer: *Acta Mater.*, 2009, vol. 57, pp. 4304–11.
41. D. Wolf: *J. Mater. Research*, 1990, vol. 5, pp. 1708–30.
42. C.S. Kim and G.S. Rohrer: *Interface Sci.*, 2004, vol. 12, pp. 19–27.
43. Q. Fan: *J. Applied Crystall.*, 2012, vol. 45, pp. 1303–08.
44. F. Heidelbach, H.R. Wenk, S.R. Chen, J. Pospiech, and S.I. Wright: *Mater. Sci. Eng. A*, 1996, vol. 215, pp. 39–49.
45. M.N. Kelly, K. Glowinski, N.T. Nuhfer, and G.S. Rohrer: *Acta Mater.*, 2016, vol. 111, pp. 22–30.
46. K. Pettersen and N. Ryum: *Metall. Mater. Trans. A*, 1989, vol. 20, pp. 847–52.